NIH Public Access
Author Manuscript
Biochim Biophys Acta. Author manuscript; available in PMC 2009 July 15.

Published in final edited form as:
Biochim Biophys Acta. 2008 April ; 1778(4): 1079–1090. doi:10.1016/j.bbamem.2008.01.024.

Characterization of lipid domains in reconstituted porcine lens membranes using EPR spin labeling approaches

Marija Raguz[a], **Justyna Widomska**[a], **James Dillon**[b], **Elizabeth R. Gaillard**[c], and **Witold K. Subczynski**[a,*]

[a]Department of Biophysics, Medical College of Wisconsin, Milwaukee, Wisconsin 53226, USA

[b]Department of Ophthalmology, Columbia University, New York, New York 10032, USA

[c]Department of Chemistry and Biochemistry, Northern Illinois University, DeKalb, Illinois, 60115,USA

Abstract

The physical properties of membranes derived from the total lipid extract of porcine lenses before and after the addition of cholesterol were investigated using EPR spin-labeling methods. Conventional EPR spectra and saturation-recovery curves indicate that the spin labels detect a single homogenous environment in membranes before the addition of cholesterol. After the addition of cholesterol (when cholesterol-to-phospholipid mole to mole ratio of 1.55–1.80 was achieved), two domains were detected by the discrimination by oxygen transport method using a cholesterol analogue spin label. The domains were assigned to a bulk phospholipid-cholesterol bilayer made of the total lipid mixture and to a cholesterol crystalline domain. Because the phospholipid analogue spin labels cannot partition into the pure cholesterol crystalline domain, they monitor properties of the phospholipid-cholesterol domain outside the pure cholesterol crystalline domain. Profiles of the order parameter, hydrophobicity, and oxygen transport parameter are identical within experimental error in this domain when measured in the absence and presence of a cholesterol crystalline domain. This indicates that both domains, the phospholipid-cholesterol bilayer and the pure cholesterol crystalline domain, can be treated as independent, weakly interacting membrane regions. The upper limit of the oxygen permeability coefficient across the cholesterol crystalline domain at 35°C had a calculated value of 42 cm/s, indicating that the cholesterol crystalline domain can significantly reduce oxygen transport to the lens center. This work was undertaken to better elucidate the major factors that determine membrane resistance to oxygen transport across the lens lipid membrane, with special attention paid to the cholesterol crystalline domain.

Keywords

lens lipids; cholesterol domain; oxygen transport; cholesterol; membrane; spin label; EPR

© 2008 Elsevier B.V. All rights reserved.

*CORRESPONDING AUTHOR: Witold K. Subczynski, Department of Biophysics, Medical College of Wisconsin, 8701 Watertown Plank Road, Milwaukee, WI 53226, USA, Tel: (414) 456 4038, Fax: (414) 456 6512, E-mail: E-mail: subczyn@mcw.edu.

Publisher's Disclaimer: This is a PDF file of an unedited manuscript that has been accepted for publication. As a service to our customers we are providing this early version of the manuscript. The manuscript will undergo copyediting, typesetting, and review of the resulting proof before it is published in its final citable form. Please note that during the production process errors may be discovered which could affect the content, and all legal disclaimers that apply to the journal pertain.

NIH-PA Author Manuscript
NIH-PA Author Manuscript
NIH-PA Author Manuscript

NIH-PA Author Manuscript

NIH-PA Author Manuscript

NIH-PA Author Manuscript

1. Introduction

Cholesterol, the most prominent sterol of mammalian cells, is located predominantly in the plasma membrane, where it comprises 35–45 mol% of the total lipids. However, the cholesterol level in human fiber cell membranes is extremely high, exhibiting cholesterol-to-phospholipid mole ratios from 1 to 2 in the cortex of the lens to as high as 3 to 4 in the lens nucleus [1]. This large difference between the nucleus and the cortex indicates that during aging the cholesterol-to-phospholipid mole ratio increases [2]. Such a molecular composition of the membrane ensures its physical and chemical stability; for example, rigidity [3,4] and resistance to peroxidation [5], respectively. It also favors the formation of rafts, as well as immiscible cholesterol crystalline domains, within the membrane. Recently, rafts were isolated from fiber cell membranes of clear lenses of the human eye [6]. However, the authors indicated that the formation of the raft domains in the eye depends on raft proteins and not the lipid composition. Cholesterol crystalline domains have been observed within the fiber cell membranes of normal and cataractous human lenses [7–10]. In model membranes at high cholesterol concentration, cholesterol also forms immiscible cholesterol crystalline domains within the bulk membrane [11–17]. Epand et al. [16,18] demonstrated that these cholesterol crystalline domains are in intimate contact with phospholipids and are not present as morphologically separate structures. Mason et al. [10] have presented X-ray diffraction evidence that the cholesterol crystalline domains are part of the membrane bilayer and not physically separate crystals. Cholesterol crystalline domains are essential for normal functioning of the eye and maintaining lens transparency to visible light [7–10]. It has also been suggested that they interfere with cataractogenic aggregation of the soluble lens protein, α-crystallin, at the membrane surface [19]. Cholesterol crystalline domains have been detected in model and fiber-cell membranes by X-ray diffraction, differential scanning calorimetry, and MAS NMR [10–13,16]. Because phospholipid analogue spin labels cannot partition into the pure cholesterol crystalline domains, the study of cholesterol crystalline domains by EPR spin labeling is hindered. However, the cholesterol analogue spin labels should partition into both the cholesterol crystalline and phospholipid-cholesterol domains, allowing both regions to be probed.

Previously, we reported on the physical properties of the lipid bilayer membrane made of the total lipid extract from the fiber cell plasma membrane of the calf eye lens using different EPR approaches [4,20]. Our observations suggest that the lipid exchange rates among possible membrane domains are faster than 10 ns, and/or these domains must be forming and dispersing rapidly on a time scale shorter than 0.3 μs. Also, immiscible cholesterol crystalline domains are not detected with cholesterol analogue spin labels. The lipids of these membranes are strongly immobilized, showing a high order parameter at all depths across the lipid bilayer. Hydrophobicity and oxygen transport parameter profiles in the lens lipid membranes have a rectangular shape, with an abrupt change between the C9 and C10 positions, which is approximately where the steroid-ring structure of cholesterol reaches into the membrane. The profiles of the oxygen transport parameter indicate that the rigidity barrier, which is more significant for permeation of non-polar molecules like molecular oxygen, is located in the polar headgroup and near-surface regions of the lens lipid membrane, to the depth of the ninth carbon. In the central region of the membrane, oxygen transport is enhanced, significantly exceeding that in bulk water, which suggests the possibility of lateral transport of molecular oxygen and other small non-polar molecules along the inner core region of the membrane (referred to as “hydrophobic channeling”). These results indicate that the high cholesterol content in the total lipid extract from the fiber cell plasma membrane is responsible for the unique properties of the membrane and allow us to conclude that the entire membrane is in the liquid-ordered-like phase.

These previous studies utilized a simple membrane system prepared from the total lipid extract of the calf eye lens. Because these were young animals (less than six months old) we did not

NIH-PA Author Manuscript

NIH-PA Author Manuscript

NIH-PA Author Manuscript

expect a significant difference in the composition of the fiber cells between the cortex and nucleus, so no such fractions was made. This difference becomes important only for older animals and humans, and manifests itself in changes in phospholipid composition and, more significantly, in the cholesterol-to-phospholipid mole ratio [21]. In humans, this ratio can increase from 1 to a value as large as 4 [1,22]. In older cows, this ratio can increase from 0.5 to 2 [23]. It has been reported that the cholesterol-to-phospholipid mole ratio in the total lipid extract from calf lens membranes is close to 1 [24–27], which makes it unlikely that we were observing pure cholesterol crystalline domains in these systems.

In the present study, we have utilized the lipid extracts of fiber cell plasma membranes from young (less than six months old) pigs. This has allowed us to compare the behavior of the membranes from different species (e.g., young pig and calf). In addition, we have investigated the effects of an immiscible cholesterol crystalline domain on the physical properties of the membrane by adding excess cholesterol to the total lipid extract. It has been reported that the cholesterol-to-phospholipid mole ratio in the total lipid extract from young pig lens membranes is approximately 0.55–0.80 [28,29]. Because both the cholesterol-to-phospholipid mole ratio and the phospholipid profile change with age, the effect of varying cholesterol concentrations can be exclusively monitored by the addition of cholesterol to young lens lipid extracts. The major phospholipids in this extract are PC (29%), PE (34%), PS (11%), and sphingolipids (21%, from which 85.6% is sphingomyelin and 14.4% is dihydrosphingomyelin) [30–32]. Palmitate is the most abundant acyl chain of both sphingomyelin (30.6%) and dihydrosphingomyelin (41.6%) [31].

The saturation-recovery EPR discrimination by oxygen transport (DOT) method has been applied to detect and characterize the pure cholesterol crystalline domain within the bulk phospholipid-cholesterol membrane made of pig lens lipids in the present study. This method has already been successfully used for detection and characterization of coexisting membrane domains [33–36] (see section 2.5 for more details). In these studies, the phospholipid-type spin labels, 1-palmitoyl-2-(n-doxylstearoyl)phosphatidylcholine (n-PC, n = 5, 7, 10, 12, 14, or 16)), n-doxylstearic acid spin label (n-SASL, n = 9), and tempocholine-1-palmitoyl-2-oleoylphosphatidic acid ester (T-PC), as well as the cholesterol analogues, androstane spin label (ASL) and cholestane spin label (CSL) were utilized. Because of the overall similarity of the molecular structures of these spin labels with phospholipids and cholesterol they should to a certain degree approximate the distribution of phospholipid and cholesterol molecules between membrane domains, as well as cholesterol-phospholipid and cholesterol-cholesterol interactions in the membrane [35,37,38,39]. Figure 1 is a schematic drawing of the lens-fiber-cell-derived membrane emphasizing the distribution and positions of the lipid spin labels in the membrane domains. The phospholipid-type spin labels should partition only into the bulk phospholipid-cholesterol domain. Thus, profiles of the order parameter, hydrophobicity, and oxygen transport parameter obtained with the use of these spin labels should describe only properties of the bulk phospholipid-cholesterol domain, without “contamination” from the cholesterol crystalline domain. The cholesterol analogues should distribute between both domains. Thus, only ASL and CSL can detect and discriminate both coexisting domains. The major focus of this current work is to establish a methodological basis to detect of cholesterol crystalline domains and to obtain physical properties of the bulk phospholipid-cholesterol membrane in the absence and presence of cholesterol crystalline domains.

2. Materials and methods

2.1. Materials

Phospholipid spin labels n-PC (n = 5, 7, 10, 12, 14, or 16), T-PC, and cholesterol were obtained from Avanti Polar Lipids, Inc. (Alabaster, AL). 9-SASL, ASL, and CSL were purchased from Molecular Probes (Eugene, OR). Other chemicals, of at least reagent grade, were purchased

NIH-PA Author Manuscript

NIH-PA Author Manuscript

NIH-PA Author Manuscript

from Sigma-Aldrich (St. Louis, MO). Chemical structures of spin labels are presented in Fig. 2.

2.2. Isolation of lipids

The total lipids from the fiber cell plasma membrane of the pig eye lens were extracted based on minor modifications of the Folch procedure [32,40]. Fresh pig eyes from animals less than six months old were obtained on the day of slaughter from Pork King Packing Company (Marengo, IL). The eyes were dissected and the lenses from ~50 eyes were pooled together. The lenses were gently mashed in a 500 mL Erlenmeyer flask with the pestle from a tissue homogenizer to which ~200 mL of methanol/chloroform (2:1 v:v) mixture was added, and the slurry was stirred for 30 minutes. The sample was distributed to corex centrifuge tubes and centrifuged at 5000 rpm for 30 minutes. The supernatants were poured into a separatory funnel, and water and methanol were added so that the final ratio of methanol/chloroform/water was 1:2:1 (v:v). The chloroform layer was removed and the water layer was extracted two more times with chloroform. All of the chloroform layers were pooled, dried with $MgSO_4$, filtered, and the solvent was removed. The resultant lipid sample was a soft, white solid stored at −20° C.

2.3. Preparation of lipid bilayer membranes

The membranes used in this work were multilameller dispersions (multilamellar liposomes) made of the total lipid extract from fiber cell plasma membranes of pig eye lenses or the mixture of pig lipids with cholesterol (with the final cholesterol-to-phospholipid mole ratio of ~1.55–1.80) containing 1 mol% spin label. The membranes were prepared by the following method [4,12]: Chloroform solutions of lipids and spin label were mixed (containing ~0.5×10^{-5} mol of total lipids—for brevity we assumed the average molecular weight of phospholipids in the total lipid extract from eye lens to be 1000 Da and the cholesterol-to-phospholipid mole ratio to be in the range of 0.55–0.80 [26,27]), the chloroform evaporated with a stream of nitrogen gas, and the lipid film on the bottom of the test tube thoroughly dried under reduced pressure (about 0.1 mmHg) for 12 h. A buffer solution (0.25 mL of 10 mM PIPES and 150 mM NaCl, pH 7.0) was added to the dried lipids at 40°C and vortexed vigorously. The buffer used for the study of samples with 9-SASL was 0.1 M borate at pH 9.5. A rather high pH was chosen in this case to ensure that all SASL probe carboxyl groups were ionized in the membranes [41].

2.4. Conventional and saturation-recovery EPR

The membranes were centrifuged briefly, and the loose pellet (about 20% lipids, w/w) was used for EPR measurements. The sample was placed in a 0.6 mm i.d. capillary made of gas-permeable methylpentene polymer, TPX, and the capillary was placed inside the EPR dewar insert. It was then equilibrated with the same gas that was used for the temperature control (i.e., a controlled mixture of nitrogen and dry air adjusted with flowmeters [Matheson Gas Products model 7631H-604]) [42,43].

Conventional EPR spectra were obtained with an X-band Bruker EMX spectrometer with temperature-control accessories. Modulation amplitude of 0.5 or 1.0 G and an incident microwave power of 5.0 mW were used for measurement at the temperature range 15–45°C. To measure the hydrophobicity profiles across the membrane, the *z*-component of the hyperfine interaction tensor of the n-PC or 9-SASL, A_Z, was determined from the EPR spectra for samples frozen at −163°C, and recorded with modulation amplitude of 2 G and an incident microwave power of 2 mW [44].

The spin-lattice relaxation times (T_1s) of the spin labels were determined by analyzing the saturation-recovery signal of the central line obtained by short-pulse saturation-recovery EPR at X-band [34,45,46]. A relatively low level of observing power (8 μW, with the loop-gap

NIH-PA Author Manuscript

NIH-PA Author Manuscript

NIH-PA Author Manuscript

resonator delivering an H_1 field of 3.6×10^{-5} gauss) was used. Accumulations of the decay signals were carried out with 2048 data points on each decay. For further detail and explanation, see Ref. [4].

2.5. The DOT approach

The bimolecular collision rate between oxygen and the free radical nitroxide moiety of spin label placed at specific locations in the membrane was evaluated in terms of an oxygen transport parameter ($W(x)$). $W(x)$ was defined as

$$W(x)=T_1^{-1}(\text{air},x) - T_1^{-1}(\text{N}_2,x), \quad (1)$$

where the T_1s are the spin-lattice relaxation times of the nitroxide in samples equilibrated with atmospheric air and nitrogen, respectively [45,47]. $W(x)$ is proportional to the product of the local translational diffusion coefficient $D(x)$ and the local concentration $C(x)$ of oxygen at a "depth" x in a lipid bilayer that is equilibrated in the atmospheric air:

$$W(x)=\text{AD}(x)C(x), \quad A=8\pi pr_0, \quad (2)$$

where r_0 (about 4.5 Å) is the interaction distance between oxygen and the nitroxide radical spin-label [48,49], and p is the probability that an observable event occurs when a collision does occur and is very close to 1 [42,50,51].

When located in two different membrane domains, the spin label alone most often cannot differentiate between these domains, giving very similar (indistinguishable) conventional EPR spectra and similar T_1 values. However, even small differences in lipid packing in these domains will affect oxygen partitioning and oxygen diffusion, which can be easily detected by observing the different T_1s from spin labels in these two locations in the presence of oxygen. In membranes equilibrated with air and consisting of two lipid environments with different oxygen transport rates—fast oxygen transport (FOT) domain and slow oxygen transport (SLOT) domain—the saturation-recovery signal is a simple double-exponential curve with time constants of T_1^{-1}(air, FOT) and T_1^{-1}(air, SLOT) [33,34].

$$W(\text{FOT})=T_1^{-1}(\text{air},\text{FOT}) - T_1^{-1}(\text{N}_2,\text{FOT}) \quad (3)$$

$$W(\text{SLOT})=T_1^{-1}(\text{air},\text{SLOT}) - T_1^{-1}(\text{N}_2,\text{SLOT}) \quad (4)$$

Here "x" from Eq. 1 is changed to the two-membrane domain, FOT and SLOT, and the depth fixed (the same spin label is distributed between the FOT and SLOT domains). W(FOT) and W(SLOT) are oxygen transport parameters in each domain and represents the collision rate in samples equilibrated with air. For further detail and explanation of the DOT method, see Ref. [36].

2.6. Calculation of the membrane oxygen permeability coefficient

Knowledge of the profiles of the oxygen transport parameter (oxygen diffusion-concentration product) make it possible to calculate a significant membrane characteristic, namely the oxygen permeability coefficient across the membrane, P_M, which connects the oxygen flux across the lipid bilayer with the difference in oxygen concentration in water on each side of the bilayer.

NIH-PA Author Manuscript

NIH-PA Author Manuscript

NIH-PA Author Manuscript

The method of calculation for P_M is based on the procedure developed by Subczynski et al. [45]. The procedure for this calculation is explained in details in earlier papers [20,52].

3. Results and discussion

3.1. Saturation-recovery measurements and evaluation of the oxygen transport parameter

Saturation-recovery measurements were carried out, as described by us earlier [4], systematically as a function of the partial pressure of oxygen, the location of spin labels in the membrane, and within the temperature range of 15–45°C for the membrane made of pig lens lipids with no cholesterol added. The recovery curves were fitted by single and double exponentials and compared. No substantial improvement in the fitting was observed when the number of exponentials was increased from one, suggesting that these recovery curves can be analyzed as single exponentials. The decay time constants were determined within an accuracy of ±3%. These observations indicate the presence of a single homogenous membrane when averaged over 0.3 μs (the shortest recovery time observed here, see also Ref. [34] for more detail).

Theoretically in these membranes, three lipid environments can be expected: the bulk lipid region, the raft domain, and the cholesterol crystalline domain. Based on the observations described above, coexisting raft and bulk lipid domains are not observed with phospholipids-type spin labels, and the existence of the cholesterol crystalline domain is not detected with cholesterol-type spin labels. It is important to note that in membranes loaded with cholesterol all lipids should be in the liquid-ordered phase (see Ref. [53]). These conditions exist in the pig fiber cell plasma membrane where the cholesterol-to-phospholipid mole ratio is approximately 0.55–0.80 [28,29].

To obtain the oxygen transport parameter, in principle, two saturation-recovery measurements should be performed: one with the sample equilibrated with nitrogen and the other with air (see Eq. (1)). However, to increase the accuracy, saturation-recovery measurements were carried out systematically as a function of the partial pressure of oxygen in the equilibrating gas mixture (% air) up to 50% air, and extrapolation to 100% air was performed to obtain the oxygen transport parameter (see Eq. (1)). This process is required because accurate observation of saturation recovery becomes increasingly difficult as the oxygen partial pressure is increased due to fast relaxations. A minimum of three decay measurements were performed for each point in the plot with accuracy of the evaluation of $W(x)$ better than ±10% (see Ref. [4] for more details).

As expected, the cholesterol crystalline domain is not formed in the membrane made of pig lens lipids, presumably because the cholesterol content is too low. Cholesterol crystalline domains have been observed in model phosphatidylcholine or sphingomyelin membranes only when the cholesterol content exceeded 50 or 67 mol%, respectively [12,54,55]. The values of the oxygen transport parameter obtained with ASL are identical within experimental error to values obtained with 10-PC (data not shown). This confirms that the bulky, rigid steroid-ring structure of cholesterol reaches into the membrane to the depth of the ninth carbon because the nitroxide fragment of ASL is located just below the steroid-ring structure (see Fig. 1 and Fig 2). The values of the oxygen transport parameter obtained with CSL are similar to those obtained with 5-PC and T-PC (data not shown). This is in agreement with the localization of the nitroxide moiety of CSL in the polar headgroup region (see section 3.5 for discussion).

3.2. Discrimination of the cholesterol crystalline domain within the bulk membrane

The native cholesterol concentration in the total lipid extract from the pig eye lens membranes was low, with the cholesterol-to-phospholipid mole ratio of 0.55–0.8 [28,29]. In order to induce

NIH-PA Author Manuscript

NIH-PA Author Manuscript

NIH-PA Author Manuscript

conditions favoring formation of cholesterol crystalline domain, we added additional cholesterol to the chloroform solution of the total lipid extract to achieve the final cholesterol-to-phospholipid mole ratio of 1.55–1.8. At a similar cholesterol-to-phospholipid mole ratio cholesterol crystalline domains have been observed in other model membranes [11–17]. Restrictions for the distribution of lipid spin labels in these membranes, indicated in Fig. 1, show that only spin-labeled cholesterol analogues can discriminate these domains. Phospholipid spin labels, which should not partition into the cholesterol crystalline domain, cannot discriminate these domains. Indeed, after addition of the excess cholesterol, saturation-recovery signals for n-PCs, 9-SASL, and T-PC were single-exponential signals, both in the absence and presence of oxygen indicating, additionally, that the bulk phospholipids-cholesterol domain is homogenous. Surprisingly, CSL did not detect two environments but instead also showed single-exponential saturation-recovery signals. Only ASL in samples equilibrated with the air/nitrogen mixture showed two-exponential saturation-recovery signals (Fig. 3 and Fig 4), which indicated the presence of two environments. We assigned them to the bulk phospholipid-cholesterol bilayer and the pure cholesterol crystalline domain. This assignment was based on expected similarities between T_1 values and oxygen transport parameter values detected in membranes made of pig lens lipids and in the bulk phospholipid-cholesterol domain in membranes after the addition of cholesterol. Shorter T_1 values and greater oxygen transport parameter values detected after the addition of cholesterol were close to those detected before for lens lipids and allowed us to conclude that the domain with the greater oxygen transport parameter value is the bulk phospholipid-cholesterol domain. The remaining values were assigned as those characterizing the pure cholesterol crystalline domain (see also Fig. 3 and Fig 4). We have assumed that the cholesterol crystalline domain is embedded in the bulk phospholipids-cholesterol bilayer. However, the possibility that part of the cholesterol crystals may be free in solution cannot be excluded using the current EPR methods.

Our results are an excellent illustration of the advantages and limitations of the DOT method. To detect membrane domains, lipid spin labels (CSL and ASL, but not n-PC, 9-SASL and T-PC, Fig. 1) have to be distributed between these domains. When located in two different membrane domains, the spin label alone most often cannot differentiate between domains, giving very similar T_1 values. For example, the saturation-recovery data for ASL presented in Fig. 4 show that in the absence of oxygen the single exponential decay is observed, indicating that T_1 values in both environments are very similar. In membranes equilibrated with air and consisting of two lipid environments with different oxygen transport rates, the fast oxygen transport (FOT) domain and the slow oxygen transport (SLOT) domain, the saturation-recovery signal should be a double-exponential curve with time constants of T_1(air, FOT) and T_1(air, SLOT). This is the case with ASL, which shows double-exponential saturation-recovery signals for sample equilibrated with the air/nitrogen mixture (Fig. 3 and Fig 4). CSL cannot distinguish these domains, probably because collision rates between oxygen and the nitroxide moiety of CSL located in the polar headgroup region are similar in these two domains.

We would also like to add, that in model DMPC and POPC membranes with a cholesterol-to-phospholipid mole ratio of 2:1, the DOT method with ASL (but not with CSL) distinguished two coexisting domains (Raguz and Subczynski, unpublished data). When the cholesterol-to-phospholipid mole ratio was 1:1 or slightly lower, the saturation-recovery signal for ASL was a single-exponential demonstrating that at this low cholesterol concentration, ASL indicates a single homogenous environment. We will not discuss here EPR data for membranes containing less than 50 mol% cholesterol where coexisting liquid-ordered and liquid-disordered domains are expected; please see our recent paper [33]. Also, in membranes made from calf lens lipids with a cholesterol-to-phospholipid mole ratio is close to 1, ASL indicated a single homogenous environment [4]. However, the DOT method with ASL distinguished two coexisting domains (Raguz and Subczynski, unpublished data) in membranes prepared with a sufficient amount of cholesterol addedto the total lipid extract to achieve cholesterol-to-phospholipid mole ratios

NIH-PA Author Manuscript

NIH-PA Author Manuscript

NIH-PA Author Manuscript

of 1.5:1, 2:1, and 3:1. In domains created at a high cholesterol content (cholesterol crystalline domains), the values of the oxygen transport parameter measured with ASL were similar, indicating that the properties of these domains should be similar as well. These oxygen transport parameter values were, however, significantly lower than those observed for the second domain, the bulk phospholipids-cholesterol domain. These findings support our conclusion that the new domain, observed with ASL in the membrane made from pig lens lipids after the addition of excess cholesterol, is a cholesterol crystalline domain.

3.3. How are the properties of the bulk membrane affected by the presence of the cholesterol crystalline domain?

The distribution of phospholipid spin labels in membranes containing cholesterol crystalline domains (Fig. 1) presented unique opportunities to compare properties of the bulk phospholipid-cholesterol domain in the presence and absence of the cholesterol crystalline domain. Figure 5 shows the profiles of the order parameter obtained in membranes made of pig lens lipids before and after the addition of cholesterol at 15 and 35°C. The profiles in the absence and presence of the cholesterol crystalline domain are practically the same at 15°C. Interestingly, at 35°C the values of the order parameter measured in the membrane center are the same for both membranes; however, the difference between profiles increases with a decrease of depth in the membrane, showing that the bulk phospholipids-cholesterol bilayer is more ordered when cholesterol is added. The increase of the order parameter at the 5-PC position caused by the presence of the cholesterol crystalline domain is equivalent to the change caused by the decrease of temperature by 10°C. A weak dependence of the order parameter on temperature was observed, which is in agreement with similar measurements in calf lens membranes [4]. This is in contrast to the strong dependence observed for the pure phospholipids membranes. The structural order determined by the static measure of the trans/gauche rotomer ratio in the hydrocarbon chains with the special attention paid to the role of cholesterol has been evaluated by other groups for lens lipid membranes from human [57,58,59], bovine [7], guinea pig [60], and rabbit [61].

Figure 6 shows hydrophobicity profiles ($2A_Z$, *z* component of the nitroxide hyperfine structure) across the bulk phospholipid-cholesterol membrane in the absence and presence of the cholesterol crystalline domain. Smaller $2A_Z$ values indicate higher hydrophobicity [44]. In both membranes, the hydrophobicity profiles show a similar rectangular shape, with an abrupt increase of hydrophobicity between C9 and C10. However, $2A_Z$ values in the membrane center (positions of 10-, 12-, 14-, and 16-PC) indicate that in the presence of the cholesterol crystalline domain the center of the bulk phospholipid-cholesterol membrane is significantly less hydrophobic than in its absence. The hydrophobicity in this region decreases from the level of hexane ($\varepsilon = 2$) to the level between dipropylamine and ethyl acetate ($\varepsilon = 2–6$). A similar effect is observed close to the membrane surface (5- and 7-PC positions) where hydrophobicity decreases below the level of methanol ($\varepsilon = 35$). These interesting findings are in agreement with our earlier observation [39] that cholesterol causes a significant increase in the hydrophobicity of the lipid bilayer center when its concentration increases up to ~30 mol%. This is then followed by a moderate decrease of hydrophobicity when the cholesterol concentration increases further to 50 mol%. Addition of cholesterol (from 0 to 50 mol%) monotonically decreases membrane hydrophobicity in the region close to the membrane surface. These similarities can explain the effect of the cholesterol crystalline domain on the hydrophobicity of the bulk phospholipid-cholesterol membrane as a result of the saturation of this phospholipid bilayer with cholesterol. The initial lipid extract from the pig eye lens had cholesterol content of 35–45 mol% [28,29], and only after the addition of excess cholesterol did the phospholipid bilayer become saturated with cholesterol to its final threshold solubility 50–60 mol% [12,54,55,56]. Interestingly, the hydrophobicity profile across the membrane made of the total lipid extract from the calf lens, for which cholesterol-to-phospholipid mole

NIH-PA Author Manuscript

NIH-PA Author Manuscript

NIH-PA Author Manuscript

ratio is close to 1, is very similar to that across the membrane made of pig lens lipids after the addition of cholesterol [4]. It indicates that the calf lens membrane is more saturated with cholesterol than the pig lens membrane.

The profiles of the oxygen transport parameter for the bulk phospholipid-cholesterol membrane in the absence and presence of the cholesterol crystalline domain obtained at 15, 25, and 35° C are presented in Fig. 7. All profiles have a rectangular shape with an abrupt increase of the oxygen transport parameter between the C9 and C10 positions. This abrupt increase is as large as 2–3 times, and the overall change of the oxygen transport parameter across the membrane becomes as large as 5–7 times. The oxygen transport parameter from the membrane surface to the depth of the ninth carbon is as low as in gel-phase PC membranes, and at locations deeper than the tenth carbon, as high as in fluid-phase membranes [35,45,47,52]. Profiles for the bulk phospholipid-cholesterol membrane in the absence and presence of the cholesterol crystalline domain are practically identical. They are also very similar to those for the membrane made of calf lens lipids and for the liquid-ordered-phase membrane made from the equimolar mixture of 1-palmitoyl-2-oleoylphosphatidylcholine (POPC) and cholesterol [4] and DMPC and cholesterol [35]. These similarities are in fact supportive of the hypothesis that the physical properties of the bulk phospholipid-cholesterol membrane are a result of the saturation of this phospholipid bilayer with cholesterol (see also Ref. [4] for more detail). It should be noted that the oxygen transport parameter is a useful monitor of membrane properties that report on translational diffusion of small molecules. However, the molecular structural properties measured using the trans/gauche rotomer ratio in the hydrocarbon chains depend on lipid composition and lipid saturation [3,58,62].

3.4. Oxygen permeability across the bulk phospholipids-cholesterol membrane

To analyze the oxygen transport across the membrane made of pig lens lipids, we constructed Fig. 8 in which $W(x)^{-1}$, a measure of resistance to oxygen permeation, is plotted as a function of the distance from the membrane center. $W(x)^{-1}$ is the reciprocal of the oxygen transport parameter and values were taken from the profile presented in Fig. 7 for 35°C. It can be seen that in the bulk phospholipid-cholesterol membrane, in both the absence and presence of the cholesterol crystalline domain, a rather high permeability barrier for oxygen transport is located in the polar headgroup region and in the hydrocarbon region to the depth of the ninth carbon, which is approximately where the rigid steroid-ring structure of cholesterol reaches into the membrane [63]. The resistance to oxygen permeation in this region is much higher than the resistance in the water phase, as indicated by the broken line in Fig. 8. However, resistance to oxygen permeation in the membrane center decreases by a factors of 5 to 7 and becomes much less than the resistance in the water phase. Although profiles of the resistance in both membranes are very similar, the steepness of the profile obtained in the presence of the cholesterol crystalline domain is significantly greater. The greater steepness indicates that the vertical fluctuations of all membrane components are decreased and the rigid plate-like portion of all cholesterol molecules are aligned at the same depth of the ninth carbon in the alkyl chains [4]. Similar observations were also made when profiles of the resistance to oxygen transport in membranes made of calf lens lipids and equimolar mixture of POPC and cholesterol were compared [20]. At physiological temperatures the steepness was greater for POPC/cholesterol membranes containing a single phospholipid, as compared with phospholipid mixture in lens lipid membranes, indicating greater alignment of cholesterol molecules in single phospholipid membranes.

The oxygen permeability coefficient, P_M, across the membrane made of pig lens lipids was estimated at 15, 25, and 35°C and compared with that estimated at 15, 25, 35, and 40°C for the membrane in which the cholesterol crystalline domain was induced. P_M values are presented in Table 1. At all temperatures, the P_M for membrane in the absence and presence of the

NIH-PA Author Manuscript

NIH-PA Author Manuscript

NIH-PA Author Manuscript

cholesterol crystalline domain is practically the same. The P_M obtained for the calf lens membrane [20] for the same temperature range is only slightly greater than that obtained for the pig lens membrane in the present work. When compared with the oxygen permeability coefficient across a water layer of the same thickness as the membrane, the oxygen permeability coefficient for the lens lipid membrane (pig and calf) was found to be significantly smaller only at 15 and 25°C (2.5 and 1.5 times, respectively). However, this difference decreases at 35°C and at 40°C (Table 1).

In Fig. 9, the temperature dependence of the oxygen permeability coefficient is plotted for two membrane regions; the region from the membrane surface to the depth of the ninth carbon where the major resistance to oxygen permeation is located and for the membrane center between the tenth carbons in each leaflet where oxygen transport is enhanced. To compare permeability properties of certain membrane regions with those of water, we displayed the data as a ratio of oxygen permeability across the appropriate membrane region (P'_M) to that across the water layer of the same thickness (P'_W). We observed that the center of the pig lens lipid membrane both in the absence and presence of the cholesterol crystalline domain can serves as a channel for oxygen transport with much higher oxygen permeability than water. To escape from this channel, oxygen must diffuse across high barriers with low oxygen permeability existing at both sides of the membrane. These observations most likely indicate that the presence of cholesterol crystalline domains does not affect the formation and properties of the hydrophobic channels in the bulk phospholipid-cholesterol domain of the lens membranes.

3.5. Can the EPR spin-labeling method characterize the cholesterol crystalline domain coexisting with the bulk membrane?

As indicated in Fig. 1, only the spin-labeled cholesterol analogues ASL and CSL can probe the pure cholesterol crystalline domain created within the bulk pig lens lipid membrane. The ASL showed the double-exponential saturation-recovery signal, indicating the presence of two coexisting domains and giving the values of the local oxygen transport parameter (around the nitroxide moiety of ASL) in these domains. The saturation-recovery signal of CSL is a one-exponential decay, indicating that the oxygen transport parameter around the nitroxide fragment of this spin label should be similar in both the bulk phospholipid-cholesterol domain and the cholesterol crystalline domain. In Fig. 10, the values of the oxygen transport parameter for ASL and CSL obtained in the coexisting bulk phospholipid-cholesterol and cholesterol crystalline domains are displayed as a function of temperature and compared with those obtained in the lens lipid membrane before the addition of excess cholesterol. These data indicate that in the wide range of temperatures, values monitored by ASL in the cholesterol crystalline domain are 2 to 5 times smaller than values monitored by ASL in the bulk phosphatidylcholine-cholesterol bilayer before and after the addition of cholesterol. There is a weaker dependence of the oxygen transport parameter on temperature in the cholesterol crystalline domain than in the bulk phospholipid-cholesterol domain; thus, the differences between permeability properties of the bulk phospholipid-cholesterol domain and the cholesterol crystalline domain are more pronounced at higher temperatures. The increase of the oxygen transport parameter in the bulk phospholipid-cholesterol domain after the addition of cholesterol may be the result of better alignment of cholesterol molecules at high cholesterol concentrations. As indicated above, CSL monitors the same oxygen transport parameter value in the bulk phospholipids-cholesterol and cholesterol crystalline domains, and the values in the bulk phospholipid-cholesterol domain are nearly identical in the absence and presence of the cholesterol crystalline domain.

The values of the oxygen transport parameter obtained at 35°C for ASL and CSL are displayed with the profile of the oxygen transport parameter across the bulk phospholipid-cholesterol domain coexisting with the cholesterol crystalline domain (Fig. 11). The nitroxide moiety of

NIH-PA Author Manuscript

NIH-PA Author Manuscript

NIH-PA Author Manuscript

ASL is located at the same depth as the nitroxide moiety of 10-PC which is 9.0 Å from the membrane center. To more accurately estimate the position of the nitroxide moiety of CSL, we assume that the vertical separation of the nitroxide moieties of ASL and CSL is the same as the distance between the oxygen atom and the carbon atom C20, the first carbon atom in the isooctyl chain, in the cholesterol molecule. This distance, obtained using molecular modeling techniques, was provided to us by Dr. Marta Pasenkiewicz-Gierula, and equals 11.3 Å. Thus, the nitroxide moiety of CSL is located 20.3 Å from the membrane center, which is in agreement with the average position of the –OH group of cholesterol in different model membranes [64–66]. Positions of the nitroxide fragments of ASL and CSL in the cholesterol crystalline domain are shifted toward the membrane center, as compared to their positions in the bulk phospholipid-cholesterol bilayer, and are evaluated based on the thicknesses of the pure cholesterol crystalline bilayer of 34 Å from X-ray diffraction measurements [10,11]. Vertical separations of nitroxide moieties of ASL and CSL in both membranes are the same. Values of the oxygen transport parameter obtained with ASL and CSL for the cholesterol crystalline domain allowed us to draw an approximate profile of the oxygen transport parameter across this domain.

Based on the profile of the oxygen transport parameter across the cholesterol crystalline domain (Fig. 11), the oxygen permeability coefficient for this domain was also evaluated for 15, 25, 35, and 40°C and the calculated values are presented in Table 2. Oxygen permeation across the cholesterol crystalline domain is significantly lower than that across the bulk phospholipid-cholesterol domain and water. Interestingly, this difference is greater at higher temperatures. At physiological temperatures, oxygen permeation across the cholesterol crystalline domain is about 30% less efficient than that across the bulk lens lipid membrane and two times less efficient than that across the water layer of the same thickness. These data strongly suggest that the rigid cholesterol crystalline domain can be a barrier to oxygen transport, which should help to maintain low oxygen concentration in the eye lens interior. This conclusion is supported by the fact that oxygen transport parameter values were measured outside the most rigid regions of the layer of cholesterol rings (see Fig. 1 and Fig 2) and, thus, the evaluation gives the upper limit of the oxygen permeability coefficient. Our findings should be especially significant for understanding oxygen transport and distribution in the aged lens and in the lens nucleus where the cholesterol crystalline domain can occupy as much as 50% of the fiber cell membrane. It is important to note that oxygen concentration in the lens is very low, reaching a value close to zero in the lens core [67]. Any increase in oxygen concentration is thought to be responsible for cataract formation; this could follow any type of oxidative stress which is known to contribute to caractogenesis by perturbing the structure of lens fiber cell membranes, disrupting the function of intrinsic proteins, and promoting the aggregation of cytosolic proteins (crystallines) [68].

4. Concluding remarks

Observations from conventional and saturation-recovery EPR measurements on membranes from pig lens lipids suggest that these membranes form a single homogenous environment on a time scale longer than 0.3 μs. In addition, the immiscible cholesterol crystalline domain is not detected with the cholesterol analogue spin labels. However, the cholesterol crystalline domain can be induced by the addition of excess cholesterol to the extracted lipid mixture. The unique composition of these immiscible domains and the unique distribution of lipid spin labels allow extensive information about the physical properties of the bulk phospholipid-cholesterol domain to be obtained; however, information about the cholesterol crystalline domain is limited.

The properties of the bulk phospholipid-cholesterol domain can be monitored with phospholipid analogue spin labels by measuring the alkyl chain order parameter and exhibit a

NIH-PA Author Manuscript

NIH-PA Author Manuscript

NIH-PA Author Manuscript

high rigidity that decreases gradually toward the membrane center. Interestingly, when membrane properties are measured by monitoring movement and/or concentration of small molecules like molecular oxygen or water, the properties appear to change abruptly between C9 and C10 showing low membrane fluidity and hydrophobicity to the depth of the ninth carbon and high membrane fluidity and hydrophobicity in the membrane center.

The bulk physical properties of membranes saturated with cholesterol, i.e., a cholesterol-to-phospholipid ratio close to 1, are mainly determined by the presence of the saturating amount of cholesterol and are practically independent of their phospholipid composition. This is based on our previous investigations on calf lens membrane lipid extracts [4,20] and pig lens lipid extracts in the present work, as well as on saturated and unsaturated PC membranes [4,20,35, 36,44]. Based on these investigations, we hypothesize that the cholesterol crystalline domain provides buffering capacity for cholesterol concentration in the surrounding phospholipid bilayer, keeping it at a constant saturating level and thus keeping physical properties of the membrane consistent and independent of changes in the phospholipid composition.

In one of our previous studies [20], we inferred that this domain could form a barrier to oxygen transport based on the close packing of the rigid steroid rings in the cholesterol crystalline domain. In our present work, we provided values of the oxygen transport parameter measured in the cholesterol crystalline domain and values of the oxygen permeability coefficient across the cholesterol crystalline domain. Our evaluation provides the upper limit of the oxygen permeability coefficient across this domain.

The cholesterol concentration in the lens membrane increases with age and is much higher in the lens nucleus than in the lens cortex. This present study provides important fundamental information about topographical and age-related differences in cholesterol-membrane interactions in the eye lens that should increase our understanding of the role that cholesterol plays in the lens.

Acknowledgements

This work was supported by grants EY015526, EB002052, and EB001980 of the National Institutes of Health.

References

1. Li LK, So L, Spector A. Age-dependent changes in the distribution and concentration of human lens cholesterol and phospholipids. Biochim. Biophys. Acta 1987;917:112–120. [PubMed: 3790601]
2. Truscott R. Age-related nuclear cataract: a lens transport problem. Ophthalmic Res 2000;32:185–194. [PubMed: 10971179]
3. Borchman D, Yappert MC, Afzal M. Lens lipids and maximum lifespan. Exp. Eye Res 2004;79:761–768. [PubMed: 15642313]
4. Widomska J, Raguz M, Dillon J, Gailard ER, Subczynski WK. Physical properties of the lipid bilayer membranes made of calf lens lipids: EPR spin labeling studies. Biochim, Biophys. Acta 2007;1768:1454–1465. [PubMed: 17451639]
5. Huang L, Estrada R, Yappert MC, Borchman D. Oxidation-induced changes in human lens epithelial cells 1. Phospholipids. Free Radic. Biol. Med 2006;41:1425–1432. [PubMed: 17023269]
6. Rujoi M, Jin JL, Borchman D, Tang DX, Yappert MC. Isolation and lipid characterization of cholesterol-enriched fractions in cortical and nuclear human lens fibers. Invest. Ophthalmol. Vis. Sci 2003;44:1634–1642. [PubMed: 12657603]
7. Borchman D, Cenedella RJ, Lamba OP. Role of cholesterol in the structural order of lens membrane lipids. Exp. Eye Res 1996;62:191–197. [PubMed: 8698079]
8. Jacob RF, Cenedella RJ, Mason RP. Direct evidence for immiscible cholesterol domains in human ocular lens fiber cell plasma membranes. J. Biol. Chem 1999;274:31613–31618. [PubMed: 10531368]

NIH-PA Author Manuscript

NIH-PA Author Manuscript

NIH-PA Author Manuscript

9. Jacob RF, Cenedella RJ, Mason RP. Evidences for distinct cholesterol domains in fiber cell membranes from cataractous human lenses. J. Biol. Chem 2001;276:13573–13578. [PubMed: 11278611]
10. Mason RP, Tulenko TN, Jacob RF. Direct evidence for cholesterol crystalline domains in biological membranes: role in human pathobiology. Biochim. Biophys. Acta 2003;1610:198–207. [PubMed: 12648774]
11. Bach D, Wachtel E. Phospholipid/cholesterol model membranes: formation of cholesterol crystallites. Biochim. Biophys. Acta 2003;1610:187–197. [PubMed: 12648773]
12. Epand RM. Cholesterol in bilayers of sphingomyelin or dihydrosphingomyelin at concentrations found in ocular lens membranes. Biophys. J 2003;84:3102–3110. [PubMed: 12719240]
13. Epand RM, Bach D, Borochov N, Wachtel E. Cholesterol crystalline polymorphism and the solubility of cholesterol in phosphatidylserine. Biophys. J 2000;78:866–873. [PubMed: 10653799]
14. Epand RM, Epand RF, Hughes DW, Sayer BG, Borochov N, Bach D, Wachtel E. Phosphatidylcholine structure determines cholesterol solubility and lipid polymorphism. Chem. Phys. Lipids 2005;135:39–53. [PubMed: 15854624]
15. Bach D, Borochov N, Wachtel E. Phase separation in dimyristoyl phosphatidylserine cholesterol mixtures. Chem. Phys. Lipids 1998;92:71–77.
16. Epand RM, Hughes DW, Sayer BG, Borochov N, Bach D, Wachtel E. Novel properties of cholesterol-dioleoylphosphatidylcholine mixtures. Biochim. Biophys. Acta 2003;1616:196–208. [PubMed: 14561477]
17. Collins JJ, Phillips MC. The stability and structure of cholesterol-rich codispersions of cholesterol and phosphatidylcholine. J. Lipid Res 1982;23:291–298. [PubMed: 7077143]
18. Epand RM. Preface. Biochim, Biophys. Acta 2003;1610:155–156.
19. Tang D, Borchman D, Yappert MC, Cenedella RJ. Influence of cholesterol on the interaction of α-crystallin with phospholipids. Exp. Eye Res 1998;66:559–567. [PubMed: 9628803]
20. Widomska J, Raguz M, Subczynski WK. Oxygen permeability of the bilayer membrane made of calf lens lipids. Biochim, Biophys. Acta 2007;1768:2635–2645. [PubMed: 17662231]
21. Yappert MC, Rujoi M, Borchman D, Vorobyov I, Estrada R. Glycero- versus sphingo-phospholipids: correlation with human and non-human mammalian lens growth. Exp. Eye Res 2003;76:725–734. [PubMed: 12742355]
22. Li L-K, So L, Spector A. Membrane cholesterol and phospholipids in consecutive concentric sections of human lenses. Lipid Res 1985;26:600–609.
23. Li L-K, So L. Age dependent lipid and protein changes in individual bovine lenses. Curr. Eye Res 1987;6:599–605. [PubMed: 3581878]
24. Broekhuyse RM, Kuhlmann ED. Lens membrane I. Composition of urea-treated plasma membranes of calf lens. Exp. Eye Res 1974;19:297–302. [PubMed: 4417164]
25. Broekhuyse RM, Kuhlmann ED. Lens membrane IV. Preparative isolation and characterization of membranes and various membrane proteins from calf lens. Exp. Eye Res 1978;26:305–320. [PubMed: 416964]
26. Broekhuyse RM. Membrane lipids and proteins in aging lens and cataract. Ciba Found. Symp 1973;19:135–149.
27. Roy D, Rosenfeld L, Spector A. Lens plasma membrane: isolation and biochemical characterization. Exp. Eye Res 1982;35:113–129. [PubMed: 7151881]
28. Sen PC, Krebsbach RJ, Pfeiffer DR. Persistent stimulation of lens fiber cell Na,K-ATPase by sodium thiocyanate. Exp. Eye Res 1986;43:315–327. [PubMed: 3023121]
29. Wei, X. Master of Science Thesis. Wollongong Australia: Dept. of Chemistry, University of Wollongong; 2006. Some biochemical studies on the human lens nucleus. The online version available at http://library.uow.edu.au
30. Meneses P, Greiner JV, Glonek T. Comparison of membrane phospholipids of the rabit and pig crystalline lens. Exp. Eye Res 1990;50:235–240. [PubMed: 2318270]
31. Byrdwell WC. Dual parallel mass spectrometers for analysis of sphingolipid, glycerophospholipid and plasmalogen molecular species. Rapid Commun. Mass Spectrom 1998;12:257–272.

NIH-PA Author Manuscript

NIH-PA Author Manuscript

NIH-PA Author Manuscript

32. Estrada R, Yappert MC. Regional phospholipids analysis of porcine lens membranes by matrix-assisted laser desorption/ionization time-of-flight mass spectrometry. J. Mass Spectrom 2004;39:1531–1540. [PubMed: 15578747]
33. Ashikawa I, Yin J-J, Subczynski WK, Kouyama T, Hyde JS, Kusumi A. Molecular organization and dynamics in bacteriorhodopsin-rich reconstituted membranes: Discrimination of lipid environments by the oxygen transport parameter using a pulse ESR spin-labeling technique. Biochemistry 1994;33:4947–4952. [PubMed: 8161556]
34. Kawasaki K, Yin J-J, Subczynski WK, Hyde JS, Kusumi A. Pulse EPR detection of lipid exchange between protein-rich raft and bulk domains in the membrane: Methodology development and its application to studies of influenza viral membrane. Biophys J 2001;80:738–748. [PubMed: 11159441]
35. Subczynski WK, Wisniewska A, Hyde JS, Kusumi A. Three-dimensional dynamic structure of the liquid-ordered domain in lipid membranes as examined by pulse-EPR oxygen probing. Biophys. J 2007;92:1573–1584. [PubMed: 17142270]
36. Subczynski, WK.; Widomska, J.; Wisniewska, A.; Kusumi, A. Saturation-recovery electron paramagnetic resonance discrimination by oxygen transport (DOT) method for characterizing membrane domains. In: McIntosh, TJ., editor. Methods in Molecular Biology. Vol. vol. 398. Totowa: Lipid Rafts, Humana Press; 2007. p. 143-157.
37. Cadenhead DA, Müler-Landau F. Molecular packing in steroid-lecithin monolayers part III: mixed films of 3-doxyl cholestane and 3-doxyl-17-hydroxyl-androstane with dipalmitoylphosphatidylcholine. Chem. Phys. Lipids 1979;25:329–343.
38. Presti FT, Chan SI. Cholesterol-phospholipid interaction in membranes. I. Cholesterol spin label study of phase behavior of cholesterol-phospholipid liposomes. Biochemistry 1982;21:3821–3830. [PubMed: 6291582]
39. Kusumi A, Subczynski WK, Pasenkiewicz-Gierula M, Hyde JS, Merkle H. Spin-label studies on phosphatidylcholine-cholesterol membranes: effects of alkyl chain length and unsaturation in the fluid phase. Biochim. Biophys. Acta 1986;854:307–317. [PubMed: 3002470]
40. Folch J, Lees M, Sloane Stanley GH. A simple method for the isolation and purification of total lipids from animal tissues. J. Biol. Chem 1957;226:497–509. [PubMed: 13428781]
41. Kusumi A, Subczynski WK, Hyde JS. Effects of pH on ESR spectra of stearic acid spin labels in membranes: probing the membrane surface. Fed. Proc 1982;41:1394.
42. Hyde, JS.; Subczynski, WK. Spin-label oximetry. In: Berliner, LJ.; Reuben, J., editors. Biological Magnetic Resonance. Vol. vol. 8. New York: Spin Labeling: Theory and Applications, Plenum Press; 1989. p. 399-425.
43. Subczynski WK, Felix CC, Klug CS, Hyde JS. Concentration by centrifugation for gas exchange EPR oximetry measurements with loop-gap resonators. J. Magn. Reson 2005;176:244–248. [PubMed: 16040261]
44. Subczynski WK, Wisniewska A, Yin J-J, Hyde JS, Kusumi A. Hydrophobic barriers of lipid bilayer membranes formed by reduction of water penetration by alkyl chain unsaturation and cholesterol. Biochemistry 1994;33:7670–7681. [PubMed: 8011634]
45. Subczynski WK, Hyde JS, Kusumi A. Oxygen permeability of phosphatidylcholine-cholesterol membranes. Proc. Natl. Acad. Sci. USA 1989;86:4474–4478. [PubMed: 2543978]
46. Yin J-J, Subczynski WK. Effect of lutein and cholesterol on alkyl chain bending in lipid bilayers: a pulse electron paramagnetic resonance spin labeling study. Biophys. J 1996;71:832–839. [PubMed: 8842221]
47. Kusumi A, Subczynski WK, Hyde JS. Oxygen transport parameter in membranes as deduced by saturation recovery measurements of spin-lattice relaxation times of spin labels. Proc. Natl. Acad. Sci. USA 1982;79:1854–1858. [PubMed: 6952236]
48. Fischkoff S, Vanderkooi JM. Oxygen diffusion in biological and artificial membranes determined by the fluorochrome pyrene. J. Gen. Physiol 1975;65:663–676. [PubMed: 1176942]
49. Subczynski WK, Hyde JS. The diffusion-concentration product of oxygen in lipid bilayers using the spin-label T1 method. Biochim. Biophys. Acta 1981;643:283–291. [PubMed: 6261814]
50. Hyde JS, Subczynski WK. Simulation of ESR spectra of the oxygen-sensitive spin-label probe CTPO. J. Magn. Reson 1984;56:125–130.

NIH-PA Author Manuscript

NIH-PA Author Manuscript

NIH-PA Author Manuscript

51. Subczynski WK, Hyde JS. Diffusion of oxygen in water and hydrocarbons using an electron spin resonance spin-label technique. Biophys. J 1984;45:743–748. [PubMed: 6326877]
52. Subczynski WK, Hyde JS, Kusumi A. Effect of alkyl chain unsaturation and cholesterol intercalation on oxygen transport in membranes: a pulse ESR spin labeling study. Biochemistry 1991;30:8578–8590. [PubMed: 1653601]
53. Munro S. Lipids rafts: elusive or illusive. Cell 2003;115:377–388. [PubMed: 14622593]
54. Slotte JP. Enzyme-catalyzed oxidation of cholesterol in mixed phospholipids monolayers reveals the stoichiometry at which free cholesterol clasters disappear. Biochemistry 1992;31:5472–5477. [PubMed: 1610794]
55. Brittman R, Kasireddy CR, Mattius P, Slotte JP. Interaction of cholesterol with sphingomyelin in monolayers and vesicles. Biochemistry 1994;33:11776–11781. [PubMed: 7918394]
56. Huang J, Buboltz JT, Feigenson GW. Maximum solubility of cholesterol in phosphatidylcholine and phosphatidylethanolamine bilayers. Biochim. Biophys. Acta 1999;1417:89–100. [PubMed: 10076038]
57. Borchman D, Lamba OP, Yappert MC. Structural characterization of lipid membranes from clear and cataractous human lenses. Exp. Eye Res 1993;57:199–208. [PubMed: 8405186]
58. Borchman D, Ozaki Y, Lamba OP, Byrdwell WC, Yappert MC. Age and regional structural characterization of clear human lens lipid membranes by infrared and near-infrared Raman spectroscopy. Biospectroscopy 1996;2:113–123.
59. Borchman D, Tang D, Yappert MC. Lipid composition, membrane structure relationships in lens and muscle sarcoplasmic reticulum. Biospectroscopy 1999;5:151–167. [PubMed: 10380082]
60. Borchman D, Giblin FJ, Leverenz VR, Reddy VN, Lin L-R, Yappert MC, Tang D, Li L. Impact of aging and hyperbaric oxygen in vivo on guinea pig lens lipids and nuclear light scatter. Invest. Ophthalmol. Vis. Sci 2000;41:3061–3073. [PubMed: 10967065]
61. Dean WL, Delamere ND, Borchman D, Moseley AE, Ahuja RP. Studies on lipids and the activity of Na,K-ATPase in lens fiber cells. Biochem. J 1996;314:961–967. [PubMed: 8615795]
62. Borchman D, Yappert MC. Sphingolipids in human lens membranes: an update on their composition and possible biological implications. Chem. Phys. Lipids 2004;129:1–20. [PubMed: 14998723]
63. McIntosh TJ. The effect of cholesterol on the structure of phosphatidylcholine bilayers. Biochim. Biophys. Acta 1978;513:43–58. [PubMed: 718889]
64. Pasenkiewicz-Gierula M, Rog T, Kitamura K, Kusumi A. Cholesterol effects on the phosphatidylcholine bilayer polar region: a molecular simulation study. Biophys. J 2000;78:1376–1389. [PubMed: 10692323]
65. Rog T, Pasenkiewicz-Gierula M. Cholesterol effects on a mixed-chain phosphatidylcholine bilayer: a molecular dynamics simulation study. Biochimie 2006;88:449–460. [PubMed: 16356621]
66. Rog T, Pasenkiewicz-Gierula M. Cholesterol-sphingomyelin interactions: a molecular dynamics simulation study. Biophys. J 2006;91:3756–3767. [PubMed: 16920840]
67. Eaton JW. Is the lens canned? Free Radic. Biol. Med 1991;11:207–213. [PubMed: 1937139]
68. McNulty R, Wang H, Mathias RT, Ortwerth BJ, Truscott RJW, Bassnett S. Regulation of tissue oxygen level in the mammalian lens. J. Physiol 2004;559:883–898. [PubMed: 15272034]

NIH-PA Author Manuscript

NIH-PA Author Manuscript

NIH-PA Author Manuscript

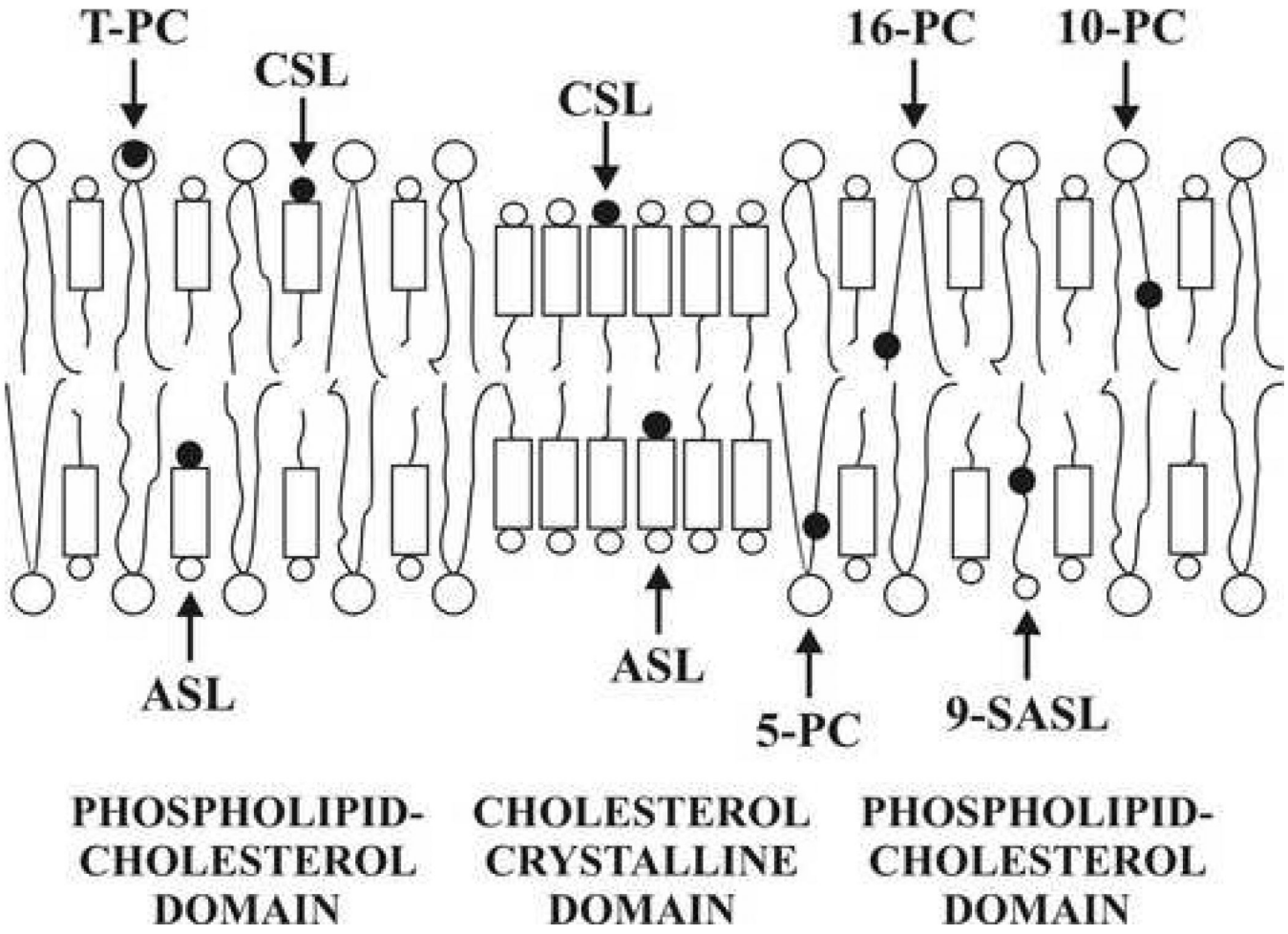

Fig. 1.

Schematic drawing of the cholesterol crystalline domain in the lens lipid membrane enriched in cholesterol. The bulk phospholipid-cholesterol and the cholesterol crystalline domains are indicated. The distribution and approximate localization of lipid spin labels in these domains is also shown. Phospholipid spin labels, 5-, 10-, 16-, T-PC and 9-SASL, are located only in the bulk phospholipid-cholesterol domain, while spin-labeled cholesterol analogue, ASL and CSL, are distributed between both domains. The nitroxide moieties of spin label are indicated as black dots.

NIH-PA Author Manuscript

NIH-PA Author Manuscript

NIH-PA Author Manuscript

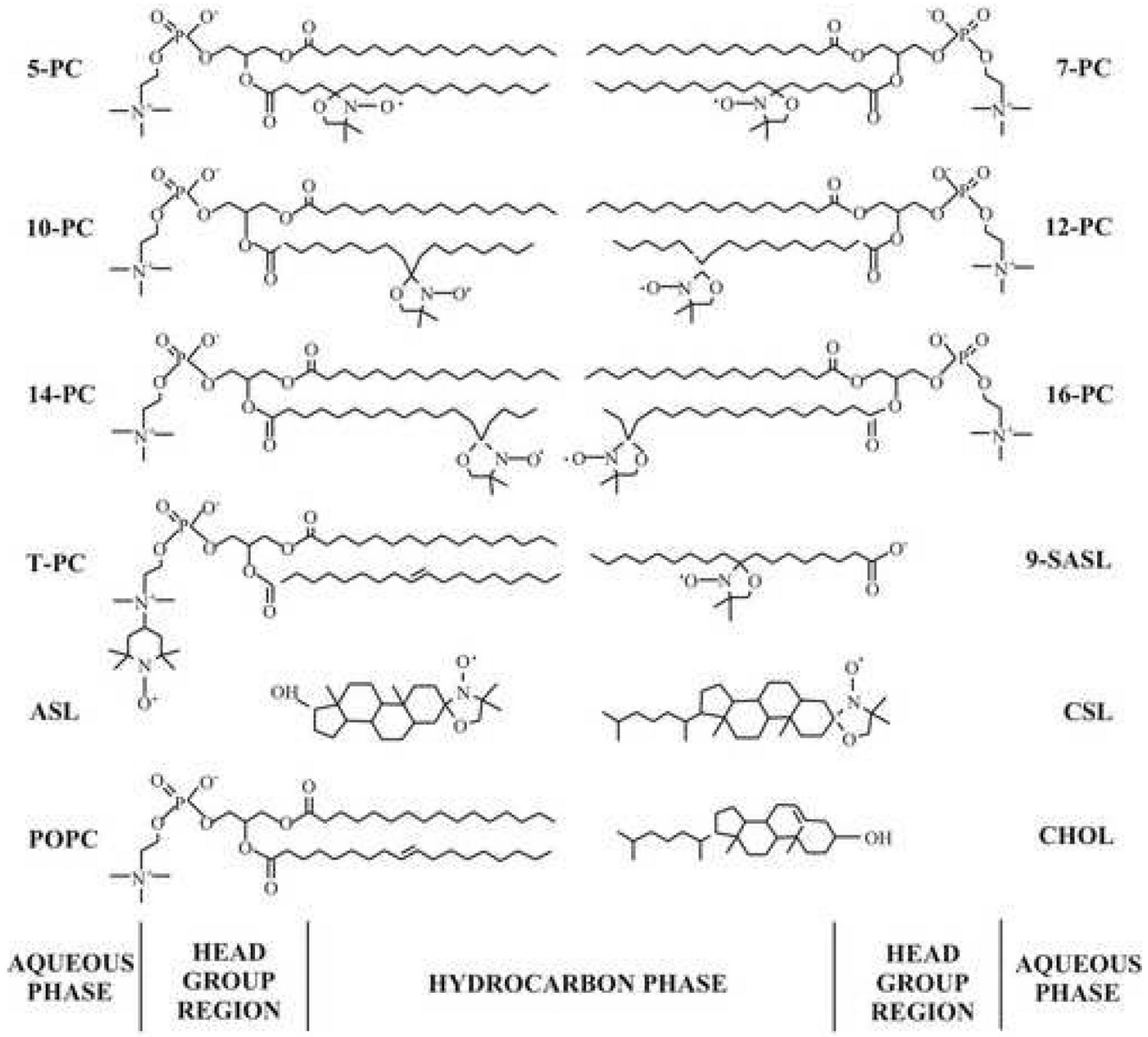

Fig. 2.

Chemical structures of spin labels used in this work. Chemical structures of cholesterol and POPC molecules are included to illustrate approximate localization of these molecules and their nitroxide moieties across the membrane.

NIH-PA Author Manuscript

NIH-PA Author Manuscript

NIH-PA Author Manuscript

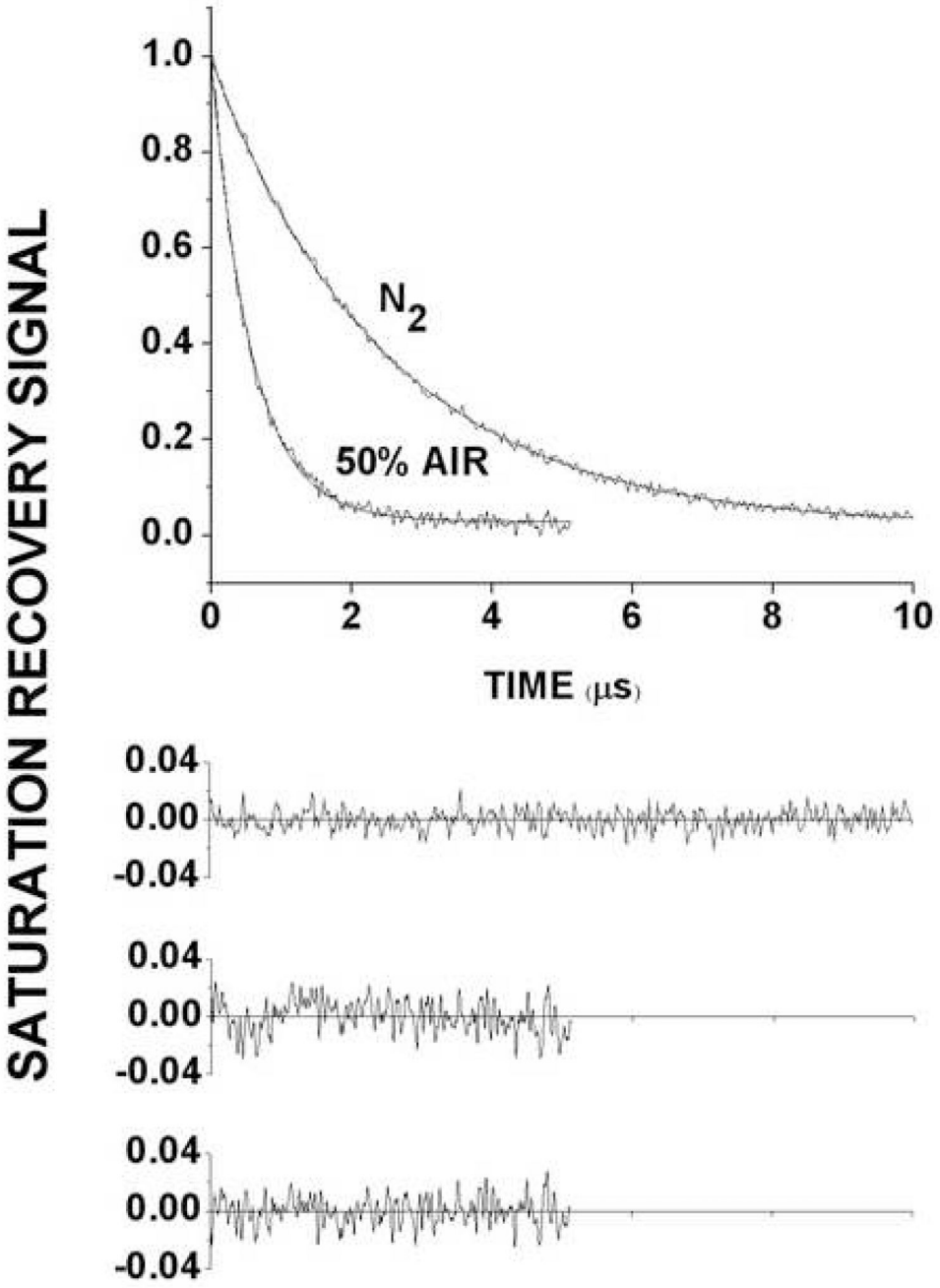

Fig. 3.

Representative saturation-recovery signals at 35°C with fitted curves and the residuals (the experimental signal minus the fitted curve) of ASL in the membrane made of lens lipids after the addition of excess cholesterol obtained in the absence and presence of oxygen. Experimental data were fitted to single exponentials with time constants 2.50 ± 0.006 μs (top) and 0.58 ± 0.34 μs (bottom) (two upper residuals). The major criterion for the goodness of a fit is the residual, indicating that a single exponential fit for a top signal is excellent. However, as shown by the residual, the fit of the bottom signal is unsatisfactory. The fit of the bottom signal to a double exponentials with time constants 1.21 ± 0.14 μs and 0.46 ± 0.02 μs is excellent (lower residual). This double-exponential fit is consistent with the presence of two immiscible

domains with different oxygen transport rate. Additional criteria for the goodness of a single and double exponential fit are explained in Ref. [34].

NIH-PA Author Manuscript
NIH-PA Author Manuscript
NIH-PA Author Manuscript

NIH-PA Author Manuscript

NIH-PA Author Manuscript

NIH-PA Author Manuscript

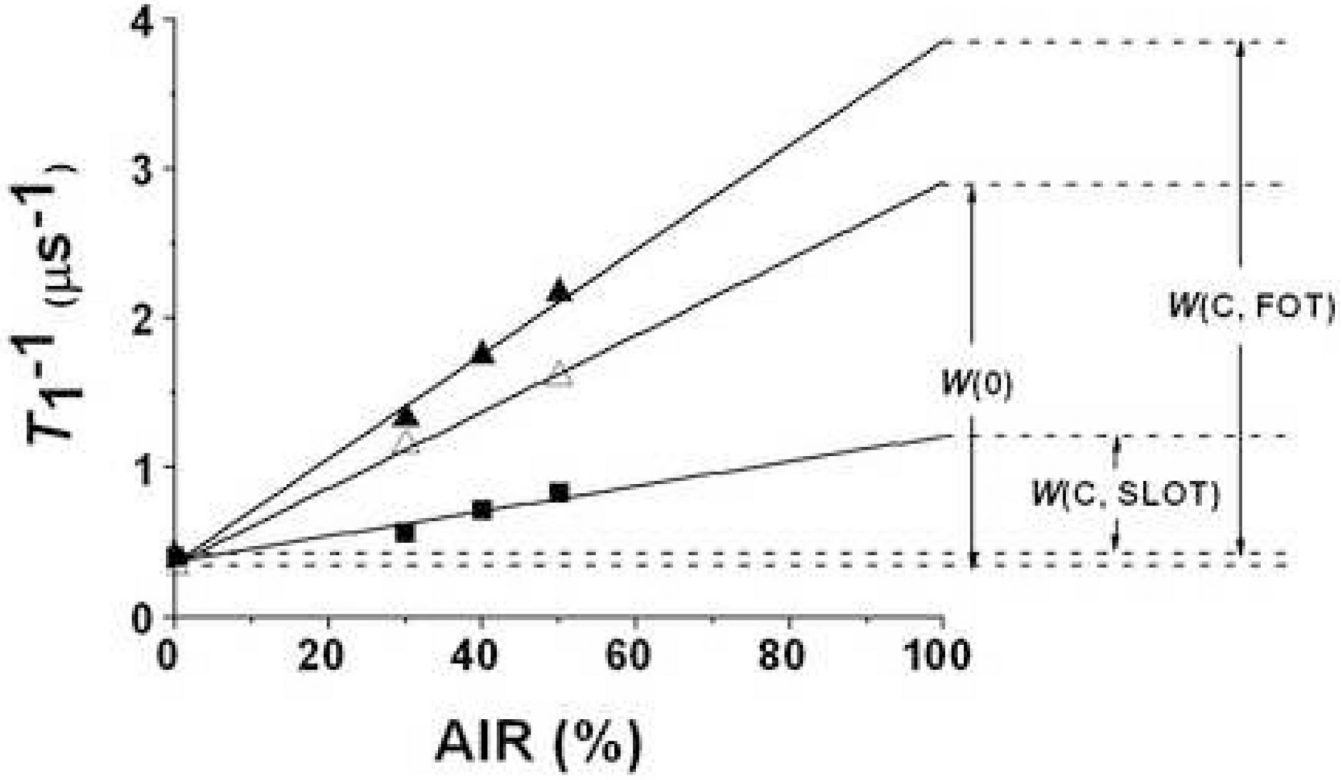

Fig. 4.

T_1^{-1} for ASL at 35°C in the membrane made of lens lipids before (Δ) and after the addition of excess cholesterol (▲,■) plotted as % air in the equilibrating gas mixture. Experimental points showed a linear dependence up to 50% air, and extrapolation to 100% air is performed to indicate a way of calculating oxygen transport parameters. *W*(0) is the oxygen transport parameter measured for the sample before addition of cholesterol. *W*(C,FOT) and *W*(C,SLOT) are oxygen transport parameters in the FOT (bulk phospholipid-cholesterol) domain and in the SLOT (cholesterol crystalline) domain obtained for the sample after addition of cholesterol from the double exponential saturation-recovery signals.

NIH-PA Author Manuscript

NIH-PA Author Manuscript

NIH-PA Author Manuscript

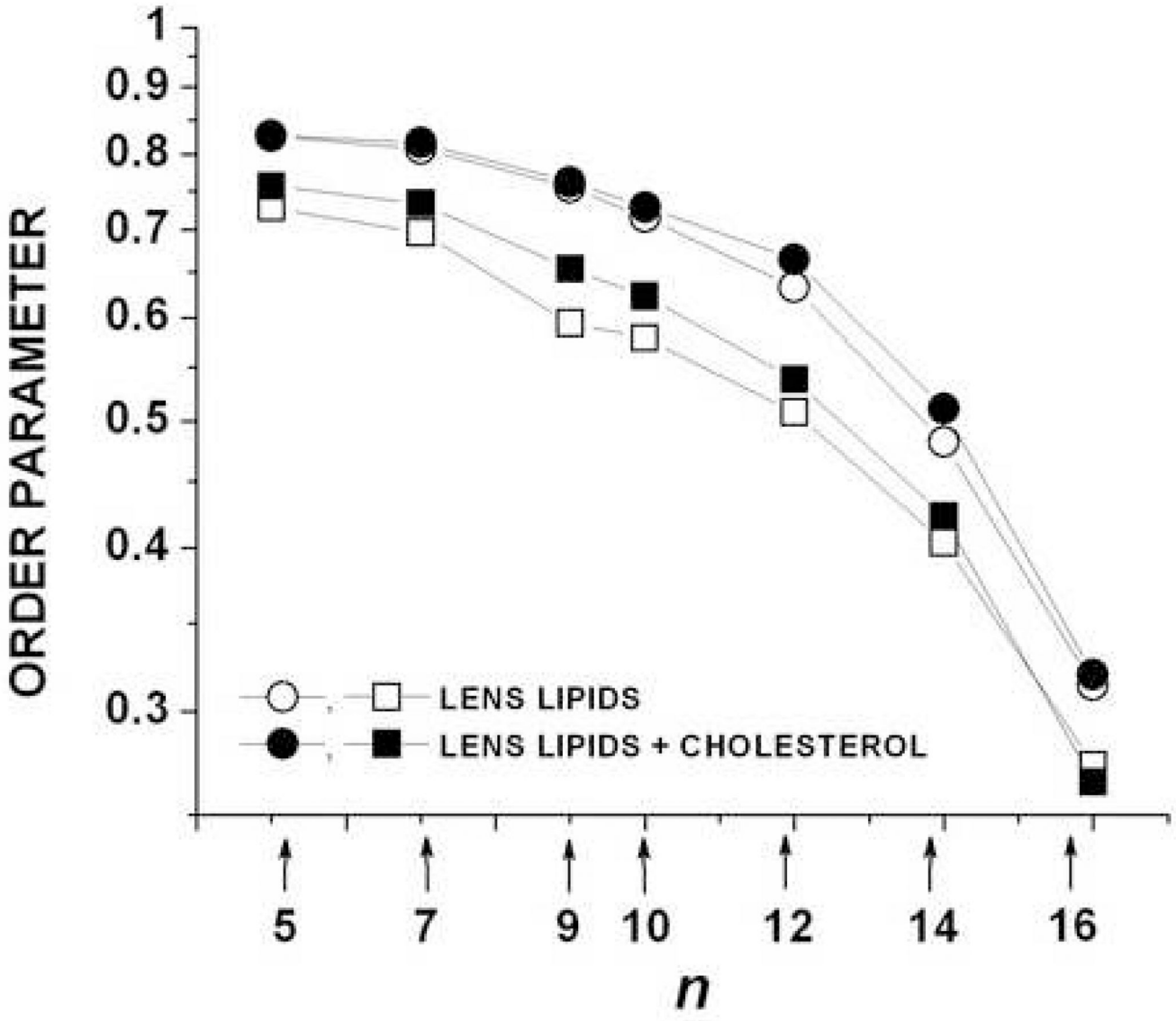

Fig. 5.

Profiles of the molecular order parameter for membranes made of lens lipids before and after the addition of excess cholesterol (order parameter is plotted in a log scale as a function of nitroxide position (n) along the alkyl chain in spin labels) at 15°C (upper curves) and 35°C (lower curves).

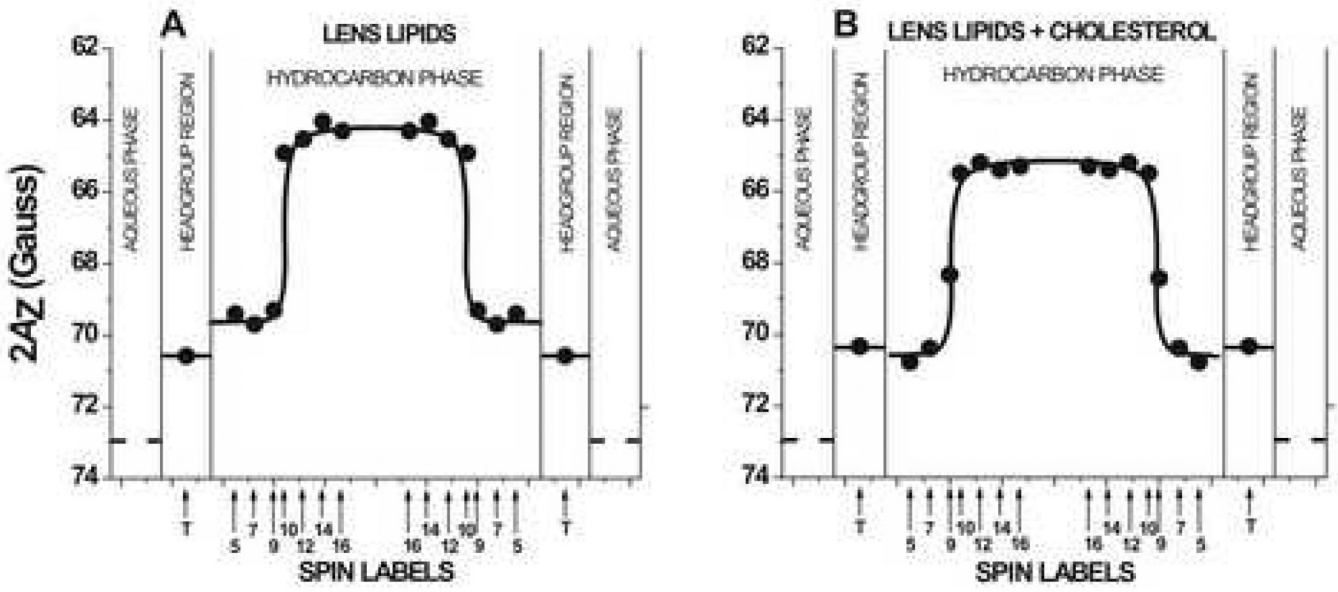

Fig. 6.

Hydrophobicity profiles ($2A_Z$) across membranes made of lens lipids before (A) and after the addition of excess cholesterol (B). Upward changes indicate increases in hydrophobicity. $2A_Z$ for 16-PC in the aqueous phase was calculated from the isotropic hyperfine constant of the nitroxide spin-label as shown in [39]. Approximate localizations of nitroxide moieties of spin labels are indicated by arrows.

NIH-PA Author Manuscript NIH-PA Author Manuscript NIH-PA Author Manuscript

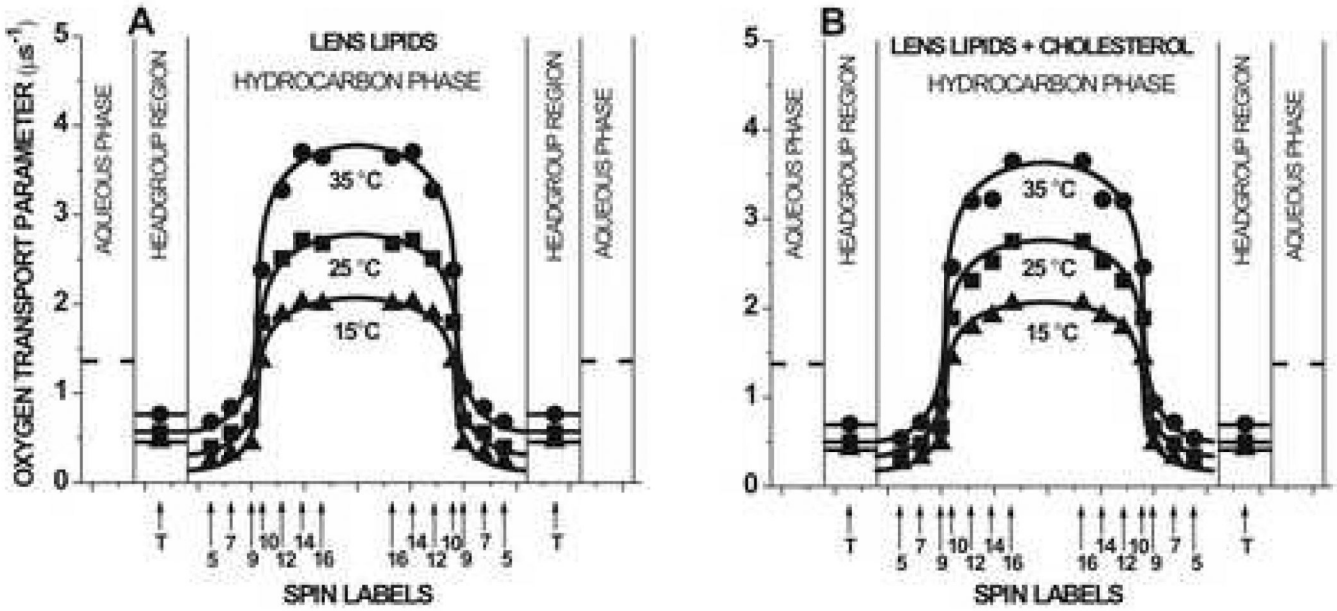

Fig. 7.

Profiles of the oxygen transport parameter across membranes made of lens lipids before (A) and after the addition of excess cholesterol (B). The broken line indicates the oxygen transport parameter in the aqueous phase. It does not change significantly because temperature dependences of oxygen diffusion and concentration are opposite. Approximate localizations of nitroxide moieties of spin labels are indicated by arrows.

NIH-PA Author Manuscript NIH-PA Author Manuscript NIH-PA Author Manuscript

NIH-PA Author Manuscript
NIH-PA Author Manuscript
NIH-PA Author Manuscript

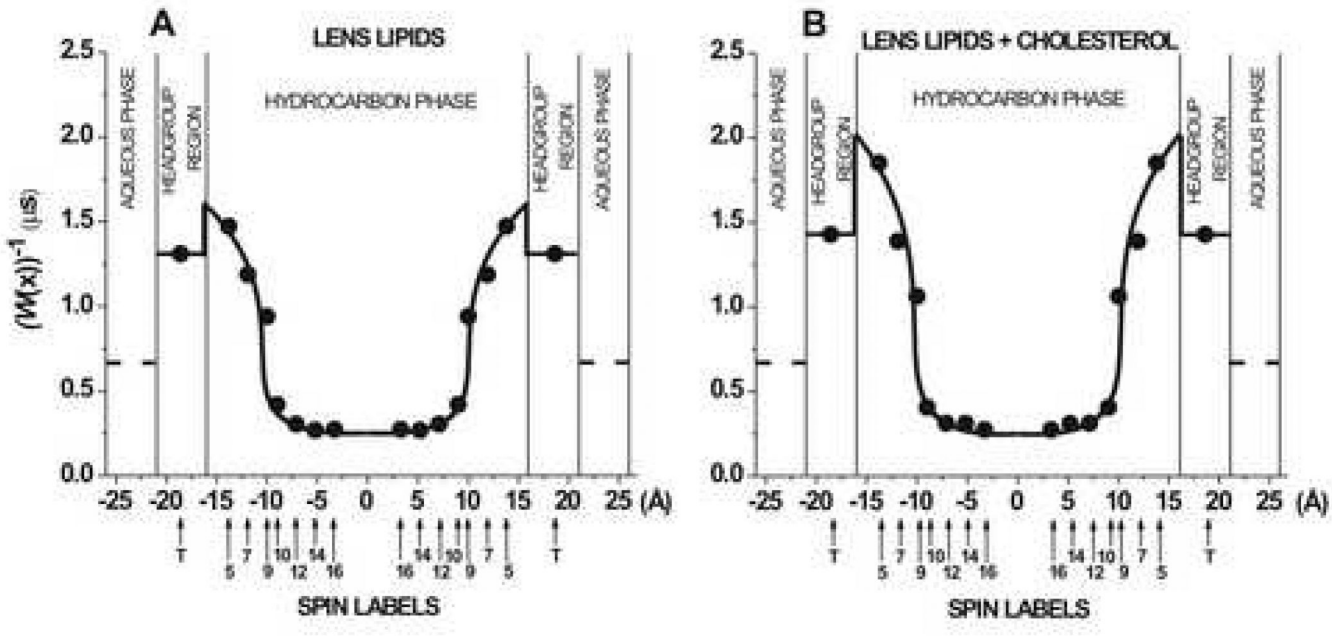

Fig. 8.

$W(x)^{-1}$ is plotted as a function of the distance from the center of the membranes made of lens lipids before (A) and after the addition of excess cholesterol (B) at 35°C to show the oxygen permeability barriers. The value of the $W(\text{water})^{-1}$, the resistance to oxygen permeation in aqueous phase, is also indicated as a broken line.

NIH-PA Author Manuscript

NIH-PA Author Manuscript

NIH-PA Author Manuscript

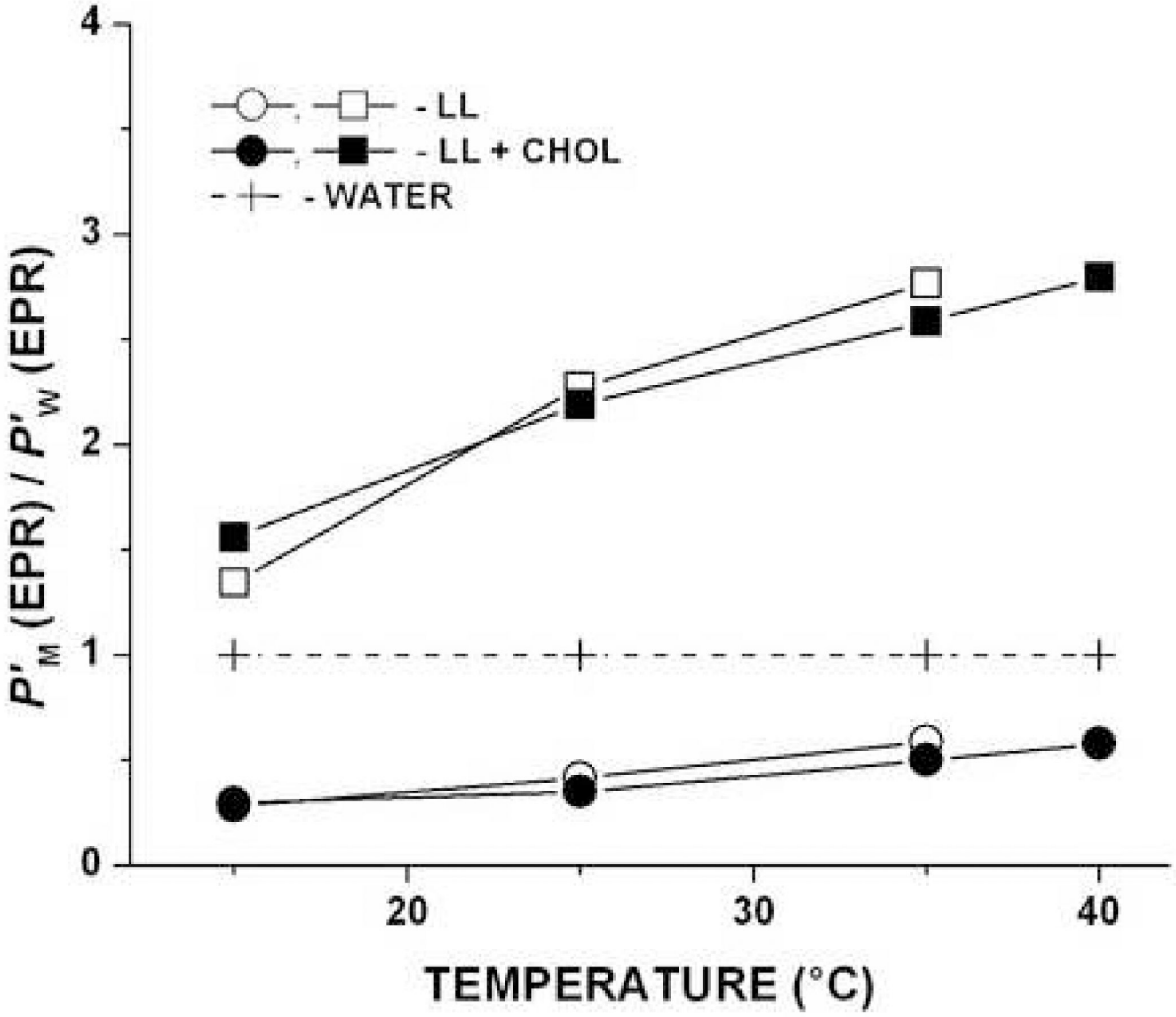

Fig. 9.

Oxygen permeability coefficient across the certain membrane region (P'_M(EPR)) relative to that across a water layer of the same thickness as the membrane region (P'_W(EPR)), i.e., P'_M(EPR)/P'_W(EPR), for lens lipids before and after the addition of excess cholesterol is plotted as a function of temperature. Both P'_M(EPR) and P'_W(EPR) were obtained by the EPR method. Two lower curves show values for the membrane region from the membrane surface to the depth of the ninth carbon (measurements with T-, 5-, 7-PC, and 9-SASL), and two upper curves show the values for the membrane region between the tenth carbons in each membrane leaflet (measurements with 10-, 12-, 14-, and 16-PC). LL-lens lipids, CHOL-cholesterol.

NIH-PA Author Manuscript

NIH-PA Author Manuscript

NIH-PA Author Manuscript

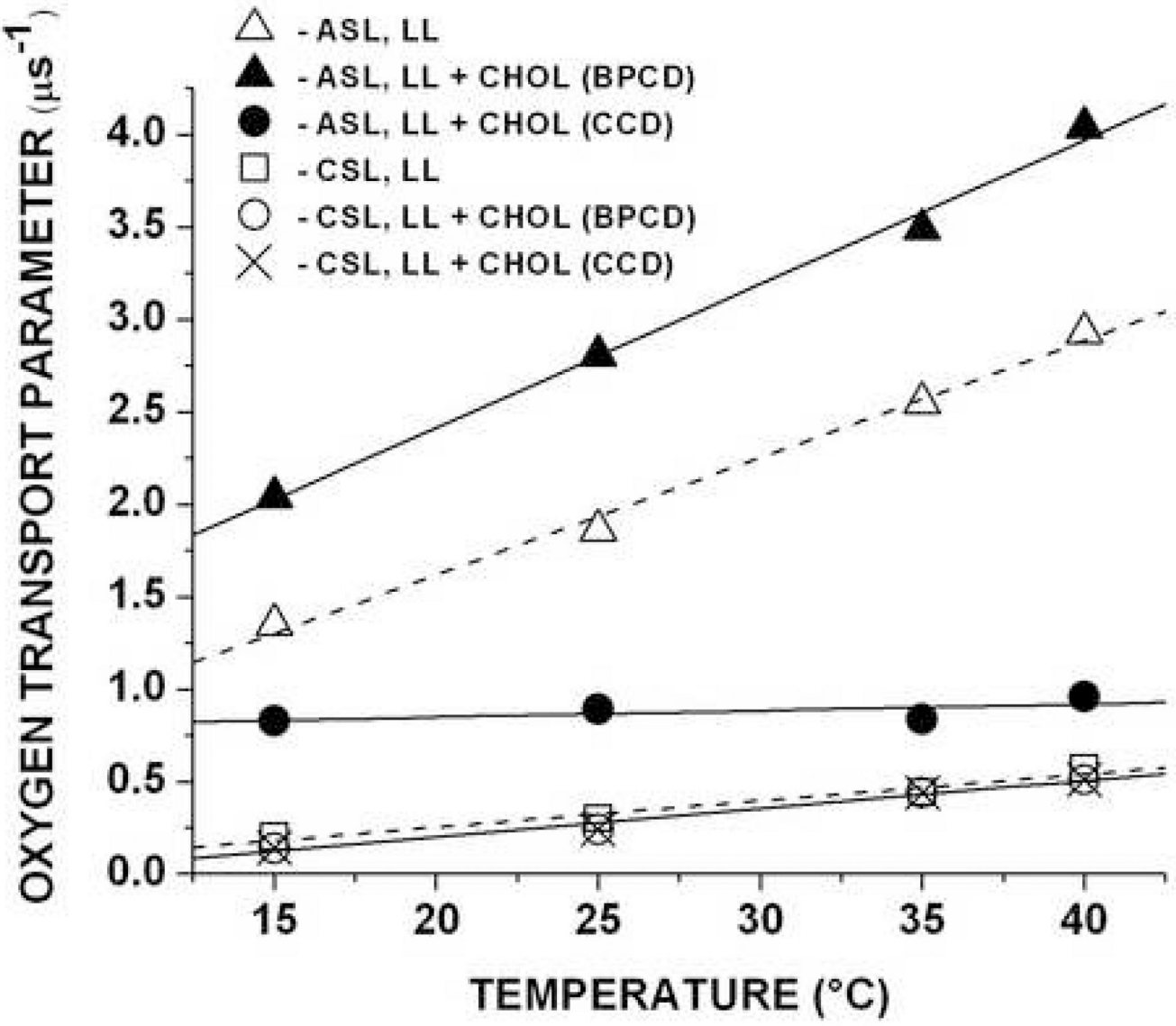

Fig. 10.

Oxygen transport parameters obtained with ASL and CSL in membranes made of lens lipids before and after the addition of excess cholesterol plotted as a function of temperature. LL-lens lipids, CHOL-cholesterol, BPCD-bulk phospholipid-cholesterol domain, CCD-cholesterol crystalline domain

NIH-PA Author Manuscript

NIH-PA Author Manuscript

NIH-PA Author Manuscript

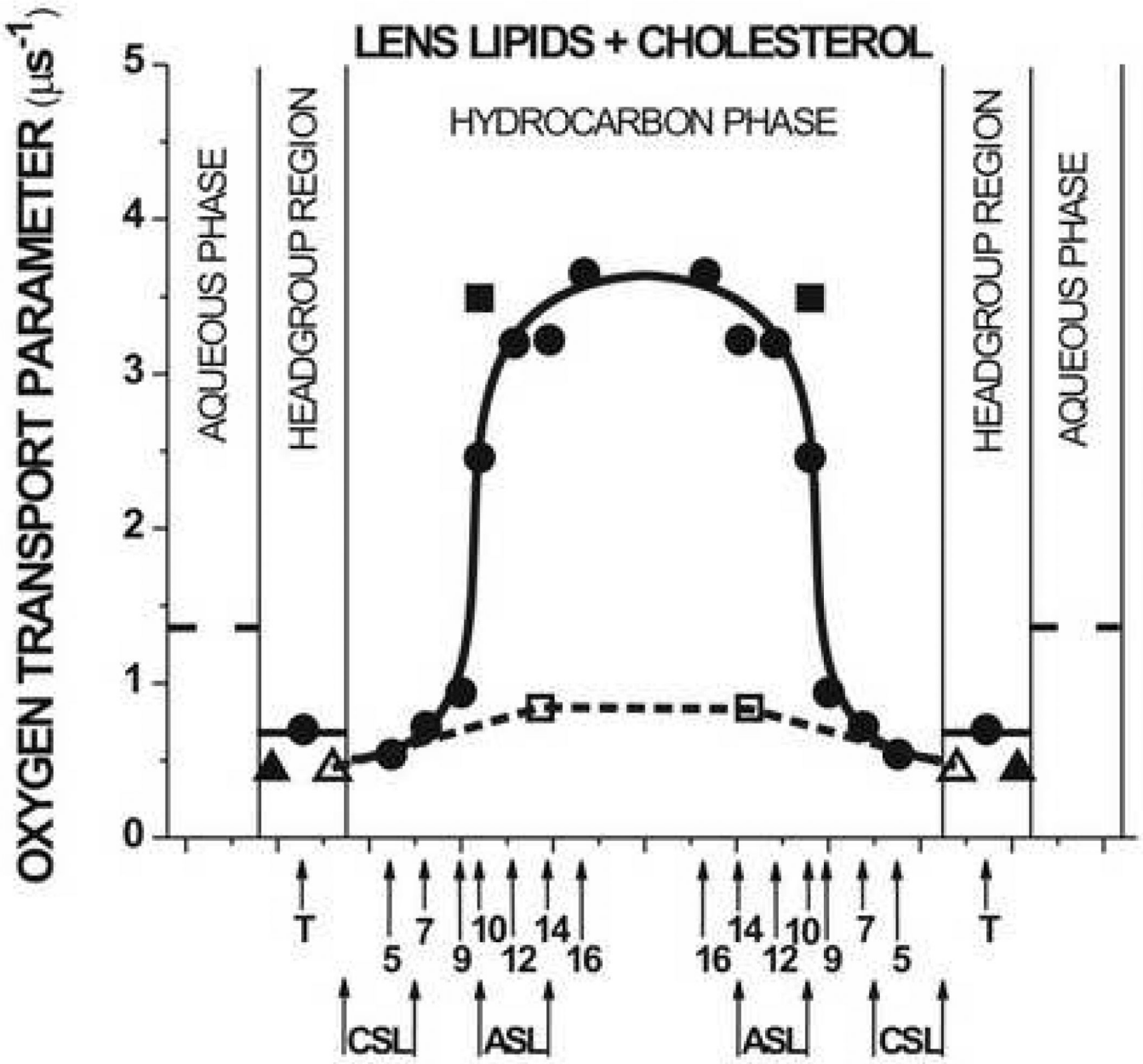

Fig. 11.

Profiles of the oxygen transport parameter across membrane domains in the membrane made of lens lipids after the addition of excess cholesterol obtained at 35°C. The profile in the bulk phospholipid-cholesterol domain (taken from Fig. 7B) with points obtained with cholesterol analogue spin labels CSL (▲) and ASL (■) located in the bulk phospholipid-cholesterol domain (taken from Fig. 10) is indicated as the solid line. The profile in the cholesterol crystalline domain obtained with cholesterol analogue spin labels CSL (Δ) and ASL (□) located in the cholesterol crystalline domain (values taken from Fig. 10) is indicated as the broken line (see section 3.5 for details).

NIH-PA Author Manuscript

NIH-PA Author Manuscript

NIH-PA Author Manuscript

Table 1

Oxygen permeability coefficients across the lens lipid membrane (bulk phospholipid-cholesterol domain) and across water layer of the same thickness as the membrane

	Oxygen permeability coefficient (cm/s)			
	15°C	**25°C**	**35°C**	**40°C**
Before the addition of cholesterol	17.9	38.3	65.1	ND[a]
After the addition of cholesterol	19.2	33.6	57.2	72.5
Across the water layer	41.3	54.6	69.3	78.8

[a]Not deffined

NIH-PA Author Manuscript

NIH-PA Author Manuscript

NIH-PA Author Manuscript

Table 2

Oxygen permeability coefficients across the cholesterol crystalline domain and across water layer of the same thickness as the cholesterol crystalline domain

	Oxygen permeability coefficient (cm/s)			
	15°C	**25°C**	**35°C**	**40°C**
Across the cholesterol domain	13.3	26.4	42.5	52.9
Across the water layer	51.2	67.7	85.9	97.7